

**AOT product over
land at the 0.6 μm
channel of the SEVIRI
sensor onboard MSG**

E. Bernard et al.

Validation of an AOT product over land at the 0.6 μm channel of the SEVIRI sensor onboard MSG

E. Bernard^{1,2}, C. Moulin², D. Ramon¹, D. Jolivet¹, J. Riedi³, and J. M. Nicolas⁴

¹HYGEOs, Euratechnologies, 165 avenue de Bretagne, 59000 Lille, France

²Laboratoire des Sciences du Climat et de l'Environnement, UMR8212, CEA-CNRS – Université de Versailles Saint-Quentin, Gif-sur-Yvette, France

³Laboratoire d'Optique Atmosphérique, UMR8518, CNRS – Université de Lille 1 – Sciences et Technologies, France

⁴ICARE Data and Services Center, Université de Lille 1 – Sciences et Technologies, France

Received: 15 April 2011 – Accepted: 12 May 2011 – Published: 24 May 2011

Correspondence to: J. Riedi (jerome.riedi@univ-lille1.fr)

Published by Copernicus Publications on behalf of the European Geosciences Union.

Title Page

Abstract

Introduction

Conclusions

References

Tables

Figures

⏪

⏩

◀

▶

Back

Close

Full Screen / Esc

Printer-friendly Version

Interactive Discussion

Abstract

The Spinning Enhanced Visible and InfraRed Imager (SEVIRI) aboard Meteosat Second Generation (MSG) launched in 2003 by EUMETSAT is dedicated to the Nowcasting applications and Numerical Weather Prediction and to provide information for climate monitoring and research. We use the data in visible and near infrared channels to derive the Aerosol Optical Thickness (AOT) over land. The algorithm is based on the assumption that the Top Of the Atmosphere (TOA) reflectance increases with the aerosol load. This is a reasonable assumption except in case of absorbing aerosols above bright surfaces. We assume that the minimum in a 14-day time series of the TOA reflectance is, once corrected from gaseous scattering and absorption, representative of the surface reflectance. The AOT and the aerosol model (a set of 5 models are used), are retrieved by matching the simulated TOA reflectance with the TOA reflectances measured by SEVIRI in its visible and Near Infra-Red (NIR) spectral bands.

The high temporal resolution of the data acquisition by SEVIRI allows to retrieve the AOT every 15 min with a spatial resolution of 3km at sub-satellite point, over the whole SEVIRI disk which covers Europe, Africa and part of South America. The resulting AOT, a Level 2 product at the same temporal and spatial resolution than SEVIRI, is presented and evaluated in this paper.

The AOT has been validated using ground based measurements from AERONET, a sun-photometer network, focusing over Europe for 3 months in 2006. The SEVIRI estimates correlate well with the AERONET measurements, $r = 0.64$, with a slight underestimate, bias = -0.017 . The sources of errors are mainly the cloud contamination and the bad estimation of the surface reflectance. The temporal evolutions exhibited by both dataset show very good agreement which allows to conclude that the AOT Level 2 product from SEVIRI can be used to quantify the aerosol content and to monitor its daily evolution with a high temporal frequency. The comparison with daily maps of MODIS AOT level 3 product shows qualitative good agreements in the retrieved geographic patterns of AOT.

AMTD

4, 3147–3198, 2011

AOT product over land at the 0.6 μm channel of the SEVIRI sensor onboard MSG

E. Bernard et al.

Title Page

Abstract

Introduction

Conclusions

References

Tables

Figures



Back

Close

Full Screen / Esc

Printer-friendly Version

Interactive Discussion

and climate models (Ghan et al., 2001; Hansen et al., 1997; Quaas et al., 2008; Schulz et al., 2006; Lohmann et al., 2010).

The direct radiative forcing due to aerosols is globally negative (-0.5 Wm^{-2} with the 5th and 95th percentiles at respectively -0.1 Wm^{-2} and -0.9 Wm^{-2} , (Forster et al., 2007)) and the first indirect effect (also called cloud albedo effect or Twomey effect) generates a decrease of the radiative forcing estimated at -0.7 Wm^{-2} with the 5th and 95th percentiles at respectively -0.3 Wm^{-2} and -1.8 Wm^{-2} (Forster et al., 2007), but again these numbers remain highly uncertain. The knowledge of microphysical parameters of tropospheric aerosol and their distribution are therefore critical for the understanding of their effect on climate (Charlson et al., 1992; King et al., 1999) and the consequence on ground and atmosphere temperatures.

Another important issue related to aerosol monitoring is the relation existing between aerosol and air quality, especially in urban areas (Health Effects Institute, 2000; Lim et al., 2004; Sifakis, 1998). The air quality domain is the study of gas (CO_2 , O_3 , NO_x ,...) and solid particle called particulate matter (PM). Many studies in particular have tried to link the aerosol optical thickness with the PM (Koelemeijer et al., 2006; Chu et al., 2003; Emili et al., 2010; Rohen et al., 2011; Wang and Christopher, 2003). For this range of application, the monitoring of aerosol loading at a high temporal resolution is important. For the anthropogenic aerosol and near the sources of emission, the time characteristic of their presence in the atmosphere is typically of one hour and the spatial variation is around 1 km (Seinfeld and Pandis, 1997; Wayne, 2000). The meteorological condition have a great influence on the stagnation and transport of the aerosol plume. Rapid variation could be detected with the high temporal resolution of SEVIRI. Grosso et al. (2007), for example, insist on the complementarity between ground air quality monitoring network which are limited in terms of spatial coverage and satellite images which cover local and regional zone.

The detection of aerosols and the study of their evolution is difficult because of their low radiative signal, their rapid temporal evolution, their interaction with molecular gases and their regional features.

AOT product over land at the 0.6 μm channel of the SEVIRI sensor onboard MSG

E. Bernard et al.

Title Page

Abstract

Introduction

Conclusions

References

Tables

Figures



Back

Close

Full Screen / Esc

Printer-friendly Version

Interactive Discussion



AOT product over land at the 0.6 μm channel of the SEVIRI sensor onboard MSG

E. Bernard et al.

[Title Page](#)[Abstract](#)[Introduction](#)[Conclusions](#)[References](#)[Tables](#)[Figures](#)[⏪](#)[⏩](#)[◀](#)[▶](#)[Back](#)[Close](#)[Full Screen / Esc](#)[Printer-friendly Version](#)[Interactive Discussion](#)

Aerosols can be detected via an estimation of their optical thickness from the surface with ground-based sun photometers like AERONET (Holben et al., 1998), or using airborne and spaceborne instrumentation. Knowledge about aerosol impacts on the environment has increased significantly with the observation from space thanks to the provision of a global coverage, long term monitoring and a good characterization of physical aerosol parameters. Several global aerosol products over land are readily available from various sensors on polar orbiting satellites such as MODIS, MERIS, MISR, AVHRR, POLDER, TOMS and OMI (King et al., 1999). If these Low Earth Orbiting (LEO) satellites can deliver rather high spatial resolution observations (around 1 km for the most of), the derived aerosol products are usually provided on a daily basis at a resolution of the order of ten kilometers or lower (MODIS, TOMS for instance). From geostationary satellites the surface sampled daily is for obvious reasons reduced and the observations spatial resolution is also lower. However the high temporal resolution is an asset with a view to monitor the diurnal cycle of the aerosol load. Another advantage is the possibility to have more than 2 retrievals per day to increase the confidence in daily or monthly products. The capability to retrieve aerosol properties from a geostationary platform and monitor their diurnal cycle has been demonstrated by Knapp (2002) and Knapp et al. (2002, 2005), using the GOES sensor. Several aerosol studies over ocean have been performed also using the Meteosat first generation satellites (Moulin et al., 1997) and the Meteosat Second Generation (MSG) (Thieuleux et al., 2005). More recent investigations have used the Spinning Enhanced Visible and InfraRed Imager (SEVIRI) sensor on-board MSG to retrieve AOT over land in the visible channel centred at 0.6 μm and noted VIS06 in the following (Popp et al., 2007; Guerrieri et al., 2007; Carrer et al., 2010; Wagner et al., 2010). All these studies showed the feasibility of retrieving the aerosol optical thickness at a time-scale ranging from 15 min (Popp et al., 2007; Guerrieri et al., 2007) to a daily average product (Carrer et al., 2010; Govaerts et al., 2010; Wagner et al., 2010).

MSG, launched by Eumetsat, is on geostationary orbit since 2003 above the Guinea Gulf and the data are available in near-real time since this date every 15 min. Thanks

AOT product over land at the 0.6 μm channel of the SEVIRI sensor onboard MSG

E. Bernard et al.

[Title Page](#)[Abstract](#)[Introduction](#)[Conclusions](#)[References](#)[Tables](#)[Figures](#)[◀](#)[▶](#)[◀](#)[▶](#)[Back](#)[Close](#)[Full Screen / Esc](#)[Printer-friendly Version](#)[Interactive Discussion](#)

to its position, the satellite is optimized to study the African, European and East of the South America continents, the Atlantic ocean and Mediterranean sea. The SEVIRI instrument is composed by 3 channels in the visible and near infrared and 8 in the thermal infrared with a spatial resolution at sub-satellite point of 3 km and a High Resolution Visible (HRV) broadband channel with a spatial resolution of 1 km at sub-satellite point. The level 1.5 data available have been corrected from radiometric and geometric non-linearity, geolocated and calibrated (Muller, 2007).

Our algorithm is based on the assumption that the Top Of the Atmosphere (TOA) reflectance in the VIS06 channel increases with the aerosol load (Fraser and Kaufman, 1985; Kaufman et al., 1997). For low surface reflectances ($\rho_g \lesssim 0.25$) and non-absorbing aerosols this hypothesis is well verified, while for absorbing aerosol models the value of ρ_g for which the assumption is still valid decreases to 0.1. Thus, the assumption is not valid for a combination of an absorbing aerosol model with a bright surface (desert, snow).

The TOA reflectance is a measurement of several contributions originating from the Earth-atmosphere system: surface, aerosols, molecules, gas and clouds. The gas and molecule contributions can be easily accounted for and corrected. The thermal IR channels allow the determination of a good cloud mask. Finally, the fixed viewing angle combined with the variable solar angles allow some angular sampling of the surface BRDF and/or aerosol phase function.

The algorithm developed aims to retrieve the aerosol optical thickness in the VIS06 channel in two steps using a method similar to the one developed for GOES-8 by Knapp et al. (2005). Over land, from a set of 14 days images, a map of estimated surface reflectance is built assuming that the darkest pixel for the period correspond to a clean-sky observation (in fact the clearest). The second step is the retrieval of the AOT for each images using these surface reflectance maps and using a set of 4 aerosol models from Omar et al. (2005) and one from WMO (Lenoble and Brogniez, 1984). Although the algorithm is dedicated to the aerosol over land retrieval, we also apply it over the ocean as a mean to test results coherence and continuity between

land and ocean.

The study we present here concerns the validation of this aerosol land product over the Europe between March and July 2006.

The algorithm generates maps every 15 min, that we validate against ground-based measurements (AERONET) for stations located in Europe. We also compare our product with data from the polar orbiting satellite MODIS, onboard Aqua and Terra, and finally analyse limits of the algorithm and give future developments to improve the quality of the AOT product.

In Sects. 2 and 3, we first present the theoretical basis of an algorithm used to retrieve aerosol optical thickness from SEVIRI observations. Then, methodology and results of the validation of this product against AERONET ground based measurements are presented and discussed in Sect. 4. The capability of the SEVIRI product to follow the aerosol diurnal cycle is illustrated through cases study and discussed against AERONET and MODIS in Sects. 5 and 6. Finally, the daily mean AOT derived from SEVIRI is also compared to AERONET over 30 days periods and the comparison with daily maps of the level 3 MODIS is performed in Sects. 7. Conclusions and main findings are summarized in Sects. 8.

2 Surface-atmosphere modelling

If L (in $\text{Wm}^{-2}\text{sr}^{-1}\mu\text{m}^{-1}$) is the radiance measured at the Top of the Atmosphere, μ_s the cosine of the solar zenith angle and E_s the constant solar irradiance, the reflectance is given by:

$$\rho = \frac{\pi \cdot L}{\mu_s \cdot E_s} \quad (1)$$

In clear-sky conditions, the atmosphere is composed by 3 main elements: gas, molecules and aerosols, which all contribute to the TOA radiance. At the wavelength considered for our retrievals, $0.6\mu\text{m}$, the main gas which participate to the absorption

AOT product over land at the $0.6\mu\text{m}$ channel of the SEVIRI sensor onboard MSG

E. Bernard et al.

Title Page

Abstract

Introduction

Conclusions

References

Tables

Figures

⏪

⏩

◀

▶

Back

Close

Full Screen / Esc

Printer-friendly Version

Interactive Discussion



AOT product over land at the 0.6 μm channel of the SEVIRI sensor onboard MSG

E. Bernard et al.

Title Page

Abstract

Introduction

Conclusions

References

Tables

Figures

◀

▶

◀

▶

Back

Close

Full Screen / Esc

Printer-friendly Version

Interactive Discussion



is the Ozone. Since we can make the assumption that this gas is located above the {molecule + aerosol} layer, we can easily dissociate the correction for this gas absorption from the rest. Regarding the {molecule + aerosol} layer mixed in the atmosphere, a coupling effect appears. The radiance of such a couple depends on many parameters: geometry, wavelength, surface pressure, aerosol type and aerosol optical thickness (Santer et al., 1999). Beyond 0.6 μm the coupling effect can be neglected (Ramon and Santer, 2001). In the aim to simplify the modelisation, molecules and aerosols are separated. Thus, the Rayleigh scattering contribution is calculated separately. Therefore, the atmospheric system we assume is divided in three separated layers: a molecular layer, located above an aerosol layer and beneath a gas absorbing layer.

The surface is considered as a Lambertian reflector for surface-atmosphere coupling term. This last point is a simplification necessary to avoid expensive computational time. Indeed, a non-lambertian surface involve the coupling between the atmospheric directional downward radiation field with the Bi-directional Reflectance Distribution Function of the target (Vermote et al., 1997) which increase the complexity of the problem. This simple hypothesis could generate uncertainties in case of inhomogeneous surface types and an important aerosol content (Vermote et al., 1997).

Under all these assumptions, the top of the atmosphere reflectance for one wavelength is given by:

$$\rho_{\text{meas}}^{\text{TOA}}(\theta_S, \theta_V, \phi) = T_g \left[\rho_{\text{Ray}}(\theta_S, \theta_V, \phi) + \rho_{\text{ag}}(\theta_S, \theta_V, \phi) \frac{T_{\text{Ray}}(\theta_S, \theta_V)}{1 - \rho_{\text{ag}} \cdot S_{\text{Ray}}} \right] \quad (2)$$

where, T_g is the gas transmittance, ρ_{Ray} , and S_{Ray} are the reflectance and spherical albedo for the Rayleigh scattering, $T_{\text{Ray}}(\theta_S, \theta_V)$ is the Rayleigh transmittance for the downward and upward directions and ρ_{ag} is the reflectance at the top of the aerosol layer, also called the aerosol-ground reflectance. These quantities depend on the solar zenith angle (θ_S), on the viewing zenith angle (θ_V) and on the relative azimuth angle (ϕ).

3 Description of the algorithm

From the native format data, the pixel counts of each channels are converted into radiances. Then, visible and near infrared channels are converted into reflectances from the Eq. (1) (Govaerts and Clerici, 2004) and brightness temperatures are computed from IR channels (IR3.9, IR8.7 IR10.8 and IR12) using the MSG report calibration (EUMETSAT, 2007).

3.1 Cloud masking scheme

Our cloud masking scheme is based on a two step process during which we first try to classify pixels among four categories using an ensemble of thresholds based test. Then, a temporal variability analysis on the High Resolution Visible and 10.8 micrometer channels is performed to refine the initial classification.

Taking example on the cloud mask developed for MODIS (Ackerman et al., 1998; Platnick et al., 2003) but adjusted to the spectral channels and spatial resolution of SEVIRI, our cloud mask is based on spectral thresholds and spatial coherence tests in the visible, near infrared and thermal infrared channels. The thresholds for the various tests have been set from detailed analysis of several scenes of SEVIRI images. As stated in Ackerman et al. (1998), the thresholds are never global but tends to represent as high a variety of situation as possible. However, the cloud detection scheme (hence the thresholds) is divided in an ocean and a land part because of the difference between the two types of surface reflectance magnitude in visible and near infrared bands. The goal of each test is to detect the probability to have a clear pixel (resp. a cloudy pixel). The value of a clear probability index (resp. a cloudy probability index) is increased if the test is achieved successfully. Finally, the respective value of both indexes determine the class of the pixel among four possible values: clear certain, clear uncertain, cloudy uncertain or cloudy certain. Cloud mask values are respectively assigned to 0, 1, 2 or 3.

AOT product over land at the 0.6 μm channel of the SEVIRI sensor onboard MSG

E. Bernard et al.

[Title Page](#)

[Abstract](#)

[Introduction](#)

[Conclusions](#)

[References](#)

[Tables](#)

[Figures](#)

[⏪](#)

[⏩](#)

[◀](#)

[▶](#)

[Back](#)

[Close](#)

[Full Screen / Esc](#)

[Printer-friendly Version](#)

[Interactive Discussion](#)



transfer code (Vermote et al., 1997). So, the transmittance is given by:

$$T_g = T_0^{\frac{m}{m_0}} \quad (3)$$

From this, we get the reflectance at the top of the atmosphere corrected from the Ozone absorption as:

$$\rho_{\text{meas}}^{\text{TOA,gas}} = \frac{\rho_{\text{meas}}^{\text{TOA}}}{T_g} \quad (4)$$

3.2.2 Rayleigh scattering correction

The reflectances are then corrected from the molecular scattering contribution in both visible channels (VIS06 and VIS08). The Rayleigh reflectance, transmittance and albedo are stored in Look-Up Tables (LUT's) calculated with the Successive Order of Scattering (SOS) radiative transfer code (Lenoble et al., 2007).

From the Eqs. (2) and (4), the TOA reflectance corrected from the Rayleigh scattering is calculated in two steps:

$$\rho_{\text{meas}}^{\text{TOA*}} = \frac{\rho_{\text{meas}}^{\text{TOA,gas}} - \rho_{\text{Ray}}}{T_{\text{Ray}}(\theta_S, \theta_V)} \quad (5)$$

then,

$$\rho_{\text{ag}} = \rho_{\text{ag}}^{\text{meas}} = \frac{\rho_{\text{meas}}^{\text{TOA*}}}{1 + S_{\text{Ray}} \rho_{\text{meas}}^{\text{TOA*}}} \quad (6)$$

This reflectance is the result of the first step of the algorithm, called the level 1B.

Title Page

Abstract

Introduction

Conclusions

References

Tables

Figures

⏪

⏩

◀

▶

Back

Close

Full Screen / Esc

Printer-friendly Version

Interactive Discussion



3.3 Estimation of the surface reference reflectance

Once the first step is achieved, a set of aerosol-ground reflectances, cloud free, is available. Aerosol contribution is separated from ground contribution using Eq. (7):

$$\rho_{\text{ag}}^{\text{sim}} = \rho_{\text{Aer}} + \rho_g \frac{T_{\text{Aer}}}{1 - S_{\text{Aer}}\rho_g} \quad (7)$$

The unknowns are the ground reflectance, ρ_g , and the 3 parameters which govern the scattering by aerosols: the reflectance (ρ_{Aer}), the spherical albedo (S_{Aer}) and the transmittance (T_{Aer}) in the upward and downward directions.

To derive the surface reflectance (ρ_g) over land, we assume that in a period of several days, the minimum of the aerosol-ground reflectance is the contribution of the surface and a residual aerosol load. As discussed previously, the method of the minimum is not valid above bright surfaces in the presence of an absorbing aerosol load (Kaufman et al., 1997). This point is discussed in Jolivet et al. (2006) showing that the TOA reflectance decreases with the increase of the AOT. So, the minimum reflectance found will not be necessarily the real TOA minimum reflectance.

Taking example on Knapp et al. (2002), a residual aerosol optical thickness of 0.03 (τ_{back}) is chosen considering the WMO continental model (see Table 1 for a description of the aerosol models). This assumption is globally realistic even if spatial and temporal variations of aerosol in the atmosphere and the spatial inhomogeneity of aerosol models can occur.

To determine the optimal period during which to look for the reference reflectance, a number of solar/satellite geometric considerations must be accounted for. During a 14 days period the solar zenith angle (θ_s) varies between 0.5 and 1.5 degrees, depending on the Earth's locations, and the azimuthal angle (ϕ) varies between -1° and 4° for the same time in the day (Jolivet et al., 2006). These variations do not lead to a significant change in the ground reflectance. However, in case of "hot spot" geometry (due to the backscattering of the sunlight by foliage), when the scattering angle (angle between the

AOT product over land at the 0.6 μm channel of the SEVIRI sensor onboard MSG

E. Bernard et al.

Title Page

Abstract

Introduction

Conclusions

References

Tables

Figures



Back

Close

Full Screen / Esc

Printer-friendly Version

Interactive Discussion



solar and viewing directions) is close to 180° rapid variations of the ground reflectance are observed. This situation occurs in Europe around the equinox.

We also assume that for such a period, surface properties (farmland, building constructions, forests,...) do not change significantly. When we consider a shorter time range of 7 days, the number of pixel kept for the estimation of the reference reflectance is 20 % lower than for a 14 days period. For a longer period, this number does not increase significantly (Jolivet et al., 2006). A similar study (Knapp et al., 2005) determines a best period of 14 days to retrieve the surface reflectance from a geostationary platform (GOES). Note that Popp et al. (2007) chose a period of 31 days for their studies but for the reasons previously mentioned this longer period may induce some severe geometrical biases.

So for each pixel of a given image (J_{day}), the algorithm looks for the day with the smallest L1B reflectance in the VIS06 channel over 14 days and considers this particular day ($J_{\text{day,ref}}$) with a minimum of aerosol load (see Fig. 1). This procedure is done for all pixels in order to construct a reference map of bi-directional reflectance valid for the scene and the time and day considered. The basis of the algorithm relies on identifying confident clear pixels so the building of this clear sky reference map is only done using “clear certain” pixels. Once every image of the day has been processed, we reconstruct the diurnal variation of the surface reflectance, for one fixed viewing zenith angle (θ_v) and several solar zenith angles (θ_s).

This pseudo-BRDF (Bidirectional Reflectance Distribution Function) is then temporally fitted with a fourth degree polynomial function to, on one hand, minimize the temporal noise due to the compositing method, and on the other hand, remove the positive bias as a consequence of a cloud contamination and negative bias because of cloud shadow. This surface reflectance is called the reference reflectance in the following of the text (Fig. 1).

The fit is done using a quality index, assigned to each pixel of every image. This index is based on several tests: pixels with no data, number of days use to find the minimum, temporal test on the presence of data and successive tests on the polynomial

AOT product over land at the 0.6 μm channel of the SEVIRI sensor onboard MSGE. Bernard et al.

[Title Page](#)[Abstract](#)[Introduction](#)[Conclusions](#)[References](#)[Tables](#)[Figures](#)[⏪](#)[⏩](#)[◀](#)[▶](#)[Back](#)[Close](#)[Full Screen / Esc](#)[Printer-friendly Version](#)[Interactive Discussion](#)

standard deviation. The quality index increases in case of the tests fail. The range is from 0 (high confidence) to 10 (low confidence).

3.4 Description of level 2 processing

3.4.1 Basis for AOT retrieval

5 Once a reference reflectance for the surface has been established, the aerosol terms (ρ_{Aer} , T_{Aer} , S_{Aer}) in the Eq. (7) remain unknown.

We simulate these terms linked to aerosols using the SOS radiative transfer code (Lenoble et al., 2007) for a range of sensor and solar zenith and azimuthal angles and aerosol optical thicknesses (varying from 0 to 2.5 with a step of 0.05) for five aerosol models in both visible channels and the NIR channel. These results are stored in Look-Up Tables (LUT's) for use during the retrieval process.

Four models are from Omar et al. (2005): moderately absorbing (MA), urban-industrial (UI), smoke (SM) and spheroidal dust (SD) (spherical shape is used to simplify calculation). They have a two-mode (accumulation and coarse mode) log-normal size distribution and their optical and geometrical features are given in the Table 1 for both of their components. This distribution is based on the median radius: few 10^{-1} μm for the coarse mode and between $5 \cdot 10^{-3}$ μm and 10^{-2} μm for the fine mode. Parameter F gives these proportions (Table 1). In addition, a fifth model from the WMO (Lenoble and Brogniez, 1984) is used, identified as a continental model, and composed of a proportion of three components: dust-like, water-soluble and soot, respectively in these proportion: 70%, 29% and 1%. In the same manner for models from Omar et al. (2005), we separated in two modes this WMO continental model with 91% for the accumulation mode and 9% for the coarse mode.

25 The single scattering albedo of each model is plotted on the Fig. 2. Three groups could be distinguished: a nearly non-absorbing model (SD), $\varpi_0 = 0.98$, a moderately absorbing group (MA + UI): $0.88 < \varpi_0 < 0.95$, and an absorbing group (WMO cont + SM): $0.9 < \varpi_0 < 0.7$. The phase function in the VIS06 channel of each model is also plotted (see Fig. 3).

AOT product over land at the 0.6 μm channel of the SEVIRI sensor onboard MSG

E. Bernard et al.

Title Page

Abstract

Introduction

Conclusions

References

Tables

Figures

◀

▶

◀

▶

Back

Close

Full Screen / Esc

Printer-friendly Version

Interactive Discussion



3.4.2 Quality assurance filters

As previously explained, the level 2 aerosol product is retrieved over the whole SEVIRI disk. However, all pixels are not directly usable because they may correspond to undetected thin clouds or cloud edges, or extreme observation geometries that usually lead to doubtful retrievals. A quality assurance mask is constructed and provided with the product to identify such situation where the aerosol inversion could be doubtful.

First of all, pixels under high viewing angles or low illumination conditions could be considered as doubtful because several assumptions made by the 6S and SOS radiative transfer developments fail under these particular geometrical conditions. Indeed, the assumption of two separated scattering layers (aerosol + molecule) used here and valid in 6S development, falls short when the solar or viewing angles are greater than 70° . In these conditions, coupling effect between aerosol particles and molecule starts to be significant and Eq. (2) does not apply anymore.

As discussed in the Sect. 3.3, the “hot spot” configuration leads to an under-estimation of the surface reflectance, due to the polynomial fit, and so, to an over-estimation of the aerosol reflectance. This scenario occurs for scattering angle close to 180° and in general is identified as a doubtful reference estimation pixel with an index reference greater than 4. But, the limit value of the angle is unclear. So, we use a rather strict upper limit of 170° scattering angle to detect the most difficult cases.

In addition, a test based on the local standard deviation of the AOT (σ_τ) is done and three classes are identified: $\sigma_\tau \leq 0.05$, $0.05 < \sigma_\tau \leq 0.1$ and $\sigma_\tau > 0.1$. Isolated pixels have a $\sigma_\tau = 0$. This test is applied on ensembles of 3 by 3 pixels and aims at removing spurious AOT values caused by presence of cloud edges or thin clouds. This rely on the assumption that spatial variability of retrieved AOT will be greater for a region partly contaminated by undetected clouds compared to only aerosols due to the more continuous nature of aerosol layers.

AOT product over land at the 0.6 μm channel of the SEVIRI sensor onboard MSG

E. Bernard et al.

Title Page

Abstract

Introduction

Conclusions

References

Tables

Figures

⏪

⏩

◀

▶

Back

Close

Full Screen / Esc

Printer-friendly Version

Interactive Discussion



4 Evaluation of the level 2 product

4.1 AERONET data

The validation is made using ground-based sun-photometers measurements of the international AErosol RObotic NETwork (AERONET) (Holben et al., 1998). We used the level 2 quality assured AOT product at 675 nm. We focussed the validation over the Europe for three months in 2006 (March, April and July), and selected 43 stations (see Table 2) for which aerosol optical thickness is available for at least one month.

4.2 Filtering the level 2 product

We use the information of the quality assurance mask to filter the level 2 aerosol optical thickness and keep the most confident pixels to compare with measurement from the ground.

Observations corresponding to a scattering angle greater than 170° are discarded and pixels viewed or illuminated under an angle greater than 70° are also rejected. Only pixels declared by the cloud mask as “clear certain” are kept for the validation to minimize contamination by potentially remaining undetected clouds.

A selection of the most confident reference reflectance pixels is done. In a general way, the relative offset between the pseudo-BRDF and the temporal fit is between 1% and 5%. A few exceptions occur at the start or the end of the day with some biases reaching 20%. We remove pixels with a reference quality index above 3.

We choose to keep the pixels with a local aerosol standard deviation (σ_τ) lower than 0.1.

4.3 Validation of the level 2 product

We present here results for the filtered AOT product over land and compare it with the AOT measured at 675 nm by AERONET. The SEVIRI pixel used for the validation is the

AOT product over land at the 0.6 μm channel of the SEVIRI sensor onboard MSG

E. Bernard et al.

Title Page

Abstract

Introduction

Conclusions

References

Tables

Figures

⏪

⏩

◀

▶

Back

Close

Full Screen / Esc

Printer-friendly Version

Interactive Discussion



one geo-located with the AERONET station. The AERONET AOT value is obtained by temporally averaging all retrievals available ± 10 min around the SEVIRI observation time.

Figure 4 shows the comparison between SEVIRI and AERONET AOT for the 3 months together and each months separately. With a total of 5637 match-up the agreement between AERONET and SEVIRI is good with a correlation coefficient of 0.64 and a linear regression with a slope of 0.8 and an intercept of 4.10^{-2} . The negative bias (AERONET – SEVIRI) of -0.017 denotes a low but global over-estimation of the AOT by the SEVIRI retrievals. This bias is between -0.03 and 0.007 for $AOT < 0.3$ and from 0.02 to 0.15 for $AOT \geq 0.3$. Note that the number of match-up N decreases with increasing AOT, with N reaching 5515 for $AOT < 0.3$ and only 122 for $AOT \geq 0.3$.

The mean relative error for $AOT < 0.1$ is high (63%) and very low ($< 5\%$) for $AOT \geq 0.1$. As seen on the density graph (Fig. 4) the bulk of the match-up are very close to the unit curve. The error is of the same order of magnitude as the estimation of the aerosol background (τ_{back}) for low AOT with a high number of correlation points. Then, the number of match-up and the error are low for high AOT. From a statistical point of view the product is satisfactory and comparable to results obtained for the MODIS algorithm (Remer et al., 2005; Levy et al., 2007).

The rather high value of the root mean square error (RMSE) (close to 0.07) traduces a large dispersion for both low and high AOT. Over-estimated SEVIRI AOT are likely due to the cloud contaminated pixels which are not detected by the cloud mask or not removed by the filtering tests. Under-estimated AOT by SEVIRI is related to the under-estimation of the background aerosol load. Also, errors on the estimate of the reference surface reflectance directly lead to an over or under estimation of AOT. Such errors are caused mostly by the temporal fit that we apply to smooth the diurnal variation of surface reference which tend to introduce systematic biases in case of local non-uniform surface configurations such as mountain slopes.

The results of the linear regression for July are the best: a correlation coefficient of 0.7, a slope of 0.9 and a low intercept (0.016). Consistent AOT until 0.4 are retrieved

AOT product over land at the 0.6 μm channel of the SEVIRI sensor onboard MSG

E. Bernard et al.

Title Page

Abstract

Introduction

Conclusions

References

Tables

Figures

⏪

⏩

◀

▶

Back

Close

Full Screen / Esc

Printer-friendly Version

Interactive Discussion

AOT product over land at the 0.6 μm channel of the SEVIRI sensor onboard MSG

E. Bernard et al.

Title Page	
Abstract	Introduction
Conclusions	References
Tables	Figures
⏪	⏩
◀	▶
Back	Close
Full Screen / Esc	
Printer-friendly Version	
Interactive Discussion	

in comparison with AERONET. Every station gives satisfying correlations except for Belsk and Chilbolton for which a large number of points over-estimate AOT compared to ground-based measurements. For April, the number of match-up is about 4 times greater than for March but the parameters of the linear regression are approximatively the same and only the bias gets improved (divided by 2). We observe high consistent values between 0.3 and 0.6 for April. The RMSE is the same for each months so denotes a constant dispersion from the measurements whatever the month.

March suffers from various problems. It is a cloudy month for Europe with a limited number of clear days available for construction of the reference (476 in March and 3291 in July). Secondly, the set of level 1 data is low: from the 2 to 5 March 2006 there is no data, and some days suffers from a lack of images. For the first period of the month, the data set for which the minimum of the TOA reflectance is looking for, is reduced from 14 days to less than 10 days (lack also of the 27 and 28 February). So, it reduces significantly the chance to observe a given pixel under clear conditions. For March, and generally for cloudy period or period with an important lack of raw data, a longer period of investigation to retrieve a clear day could be necessary. All these factors contribute to negatively impact the quality of our surface reflectance reference.

A bias is found for March which is twice that of the two other months. This is explained by a more important number of over-estimated data which could be due to the failure of the cloud mask or/and to a problem in the estimation of the reference reflectance. A strong link obviously exists between the cloud detection and the construction of a good reflectance reference and our cloud mask scheme could certainly be improved. However, over-estimation of the AOT could be due also to the under-estimation of the surface reflectance which in March could occur over Europe because of rapid change in vegetation cover. Finally, March is a period during which observations under the “hot-spot” configuration are common for Europe. The temporal fitting of the surface reflectance reference tends to smooth out this feature of the BRDF yielding a systematic under estimate of surface reflectance in this particular observation geometry. The limit value of 170° applied to the scattering angle may not be restrictive



enough in some cases and could partly contribute to this general overestimate of AOT in March. Despite this, retrievals for March are acceptable for high AOTs up to 0.4.

The main interest of SEVIRI is the high temporal frequency of observation. To illustrate this, two particular stations are considered for which the diurnal evolution of the SEVIRI AOT is plotted and compared with AERONET measurements. Cabauw (Fig. 5) and Rome (Fig. 6) are located at the North and South of Europe, with different type of surface: Cabauw is in an agricultural region and Rome Tor Vergata is located in the suburb of Rome.

A very good general monitoring is observed for both stations. The diurnal cycle is well observed by SEVIRI with an important number of retrievals per day. For Rome the daily mean absolute relative error (percent error) is between 20 % and 30 % and the bias is close to zero (0.003) except for the 14 for which SEVIRI over-estimate AERONET of 0.04. For Cabauw the relative bias ranging from 6 % to 58 %.

For instance, for Cabauw on the 1 July (Fig. 5), the maximum, in the morning, and the minimum, in the afternoon, are well retrieved by SEVIRI. The two maximum at 13:30 and 14:30 are missing in SEVIRI retrievals because they have been rejected during cloud screening. The 2 July, SEVIRI is in very good agreement with AERONET before 11:00 and after 13:00. Between these two hours, SEVIRI retrieves an aerosol optical thickness greater than 0.22 while AERONET measures an AOT of 0.15 at only two hours: 12:15 and 12:45. Visual inspection of the visible images during that timeframe revealed the presence of scattered clouds around the station which were probably too small to be detected with the spatial resolution of SEVIRI (≈ 5 km at this latitude).

In general, SEVIRI aerosol retrieval shows a good stability of the AOT from one slot to the other except in some cases like on the 20 July above Rome (Fig. 6). Between 11:00 and 14:00 the aerosol optical thickness varies between 0.1 and 0.2. From 11:15 to 11:45 the best aerosol model is successively the Moderately Absorbing (MA) and the Smoke (SM) models, and the AOT varies between 0.06 (MA) and 0.2 (SM). This change is explained by the method used to select the best model and the spectral characteristic of SEVIRI: the discrimination between the models is difficult and several

AOT product over land at the 0.6 μm channel of the SEVIRI sensor onboard MSG

E. Bernard et al.

Title Page

Abstract

Introduction

Conclusions

References

Tables

Figures

⏪

⏩

◀

▶

Back

Close

Full Screen / Esc

Printer-friendly Version

Interactive Discussion

AOT product over land at the 0.6 μm channel of the SEVIRI sensor onboard MSG

E. Bernard et al.

[Title Page](#)[Abstract](#)[Introduction](#)[Conclusions](#)[References](#)[Tables](#)[Figures](#)[⏪](#)[⏩](#)[◀](#)[▶](#)[Back](#)[Close](#)[Full Screen / Esc](#)[Printer-friendly Version](#)[Interactive Discussion](#)

In the north of France and above Benelux, a very low aerosol optical thickness is retrieved, around 0.1, confirmed by 2 AERONET stations, Lille and Cabauw, for which SEVIRI is in good agreement (Fig. 9). Above Cabauw, SEVIRI retrieves AOT equal to 0.2 between 11:00 and 12:30 while AERONET measures AOT of 0.1. Once again, scattered clouds are present around the Cabauw station during that day and may well be responsible for this bias, as suggested by the relatively high local standard deviation of the AOT which is close to the threshold of 0.1 (see Sect. 3.4.2).

Two successive AQUA overpasses on 14 July 2006 can be temporarily matched with SEVIRI observations at 12:00 UTC and 13:45 UTC. MODIS aerosol product derived from granules acquired between 12:00 and 12:10, and between 13:45 and 13:50 respectively have been aggregated to produce maps of AOT that can be directly compared to the SEVIRI derived aerosol product. MODIS aerosol optical thickness over land (Remer et al., 2005) is delivered at 660 nm under the name “Corrected_Aerosol_Optical_Depth_Over_Land”. We used the Quality Assurance (QA) index to filter pixels and keep only those with a QA = 3 as recommended by Levy et al. (2009).

The comparison with MODIS help us to confirm the presence of a large aerosol load over France and Germany. We can observe the same geographical patterns between maximum and minimum of aerosol load and clouds (black zones). MODIS seems to retrieve higher aerosol optical thickness over the region with AOT values between 0.2 and 0.6 for MODIS while they range from 0.05 to 0.5 for SEVIRI at 12:00 and 13:45. The differences could be due to the aerosol models used by the two algorithms or due to the surface reflectance estimation for which both methods are different. Obviously, MODIS takes advantage of its higher spatial resolution (between 250m and 1km) and spectral coverage to better discriminate clouds and aerosols and MODIS aerosol products have demonstrated a very good correlation with AERONET measurements (Levy et al., 2007). However, where MODIS has only two daily observations at best for a given region, SEVIRI can follow the temporal evolution of the aerosol plume in a qualitative way as will be illustrated in the following Section.

errors are calculated ($\Delta\tau > 0.9\tau$) and biases are greater than 0.04. We can reasonably say that, even if some biases exist, daily SEVIRI AOT in Fig. 11 allow to monitor the monthly variability observed by AERONET.

On the 10 and the 11 July, Rome AERONET station measures an average AOT of 0.2 and 0.18. SEVIRI is very well correlated on the 11 but retrieves an AOT of 0.1 on the 10. An analysis of the original time resolution L2 product shows that diurnal cycles are observed on these two days: AOT around 0.12–0.15 in the morning, and 0.22 to 0.3 in the afternoon (see Fig. 6). This could explain the difference between AERONET and SEVIRI daily mean AOT. On the 10, SEVIRI retrieves AOT only in the morning while in the afternoon values are discarded because they were declared as uncertain clear-sky pixels.

On the 3 April for Granada, AERONET measures a daily AOT of 0.46 with only 2 measurements at 07:00 and 07:30 while SEVIRI has no retrieval because all the pixels are declared as cloudy. On the 2 April, in the afternoon, AERONET measures also high AOT ($\tau_{\text{AER}} = 0.33$) while SEVIRI retrieves AOT between 0.3 and 0.6 but all declared as uncertain clear-sky and thus discarded. That is the same situation on the 4 April.

Pixels with valid values are retrieved by SEVIRI but considered as doubtful (uncertain clear-sky) or cloudy.

These two examples show the importance of the cloud mask and the difficulty to avoid wrong identification between clear-sky and cloudy pixels.

For the four stations of interest, the mean number of individual level 2 AOT used to calculate a daily AOT is greater than 4. In March, this value reaches 5 for Le Fauga and Rome, and 8 for Fontainebleau and Granada. In July, this value is ranging from 7 (Fontainebleau) to 13 (Le Fauga and Rome). This SEVIRI product thus provides daily AOT which are much more representative than polar orbiting sensors such as MODIS because they allow only two measurements per day at best. It is noteworthy that the number of individual AOT used to compute the daily mean from SEVIRI is usual comparable to that of AERONET.

AOT product over land at the 0.6 μm channel of the SEVIRI sensor onboard MSG

E. Bernard et al.

Title Page

Abstract

Introduction

Conclusions

References

Tables

Figures

⏪

⏩

◀

▶

Back

Close

Full Screen / Esc

Printer-friendly Version

Interactive Discussion

Globally, SEVIRI AOT retrievals monitor very well the AOT measured by AERONET and allow a satisfactory monitoring of its variability.

7.2 Comparison with MODIS L3 maps

We processed daily averaged maps from the SEVIRI L2 filtered product. We compared these maps with the MODIS AQUA level 3 daily AOT product at $0.6\ \mu\text{m}$ (file type MYD08 and collection 051, (Hubanks et al., 2008)).

The original projection of MODIS is rectangular with a spatial resolution of 1° . The MODIS product chosen to compare is the corrected and screened AOT in the $0.66\ \mu\text{m}$ channel above land and the effective AOT above ocean. It is the most confident L3 product available (Levy et al., 2009) because it includes an averaged AOT weighted by the confidence index.

Our L3 SEVIRI product has been projected on a rectangular grid with a resolution of 0.1° which is close to the original SEVIRI radiance data over Europe.

Figure 12 shows daily maps from the 17 to the 20 July 2006. These Figures shows the main differences between the two products: MODIS allows to retrieve AOT at high latitudes where SEVIRI is limited by the viewing zenith angle (large air masses). However, SEVIRI products are made of several original images which reduces the cloud cover and are not affected by the inter-orbital gaps like MODIS.

Another main feature shown in Fig. 12 is the very low level of noise in our SEVIRI product compared to that of MODIS, particularly around cloudy areas (e.g. over France and Spain on the 19 July on Fig. 12). This is due to the facts that our cloud mask is very restrictive and that SEVIRI AOT are computed using several pixels in the day, which limits the impact of contaminated pixels.

For these 4 days an aerosol event coming from the North of Africa (17 July) crosses Europe and reaches the North West of Europe on the 20 July. It is a frequent event that seasonal dust transport coming from the Sahara fly over the Mediterranean sea (Moulin et al., 1997). Both sensors allow to monitor very well this event.

AOT product over land at the $0.6\ \mu\text{m}$ channel of the SEVIRI sensor onboard MSG

E. Bernard et al.

Title Page

Abstract

Introduction

Conclusions

References

Tables

Figures

⏪

⏩

◀

▶

Back

Close

Full Screen / Esc

Printer-friendly Version

Interactive Discussion



AOT product over land at the 0.6 μm channel of the SEVIRI sensor onboard MSG

E. Bernard et al.

Title Page

Abstract

Introduction

Conclusions

References

Tables

Figures

⏪

⏩

◀

▶

Back

Close

Full Screen / Esc

Printer-friendly Version

Interactive Discussion



channel. This assumption is valid except above bright surfaces in the presence of absorbing aerosols. Then, to derive the surface reflectance in the VIS06 channel, we assume that over a period of 14 days the minimum of the Ozone and Rayleigh corrected TOA reflectance is the contribution of the surface reflectance and an aerosol background. By assuming that the aerosol background is low and equal to 0.03, we estimate the surface reflectance. This estimation of the surface reflectance also relies on the assumption that the property of land does not change significantly during 14 days and that the solar angles (zenithal and azimuthal) vary slightly (from 1° to 4°).

The AOT at 0.6 μm is retrieved using Look-Up-Tables (LUT's) for 5 aerosol models. With the VIS08 (0.8 μm) and NIR16 (1.6 μm) channels, the best model is chosen by iteratively calculating the difference between measured and simulated reflectances at these two wavelengths.

The level 2 AOT is filtered to avoid non-favourable geometrical and clouds configurations in order to remove the maximum of spurious retrievals.

We compared this L2 product with in-situ AERONET measurements at 0.675 μm and validated the AOT above Europe for 3 months of 2006. The final set contains more than five thousands match-up and the correlation is good between the two datasets ($r = 0.64$). SEVIRI tends to slightly over-estimate AOT compared to AERONET with a positive bias of 0.017. The relative error and the size of the sample decrease drastically between low and high AOT: 63 % for $\tau < 0.1$ with $N = 2557$ and less than 1 % for $\tau \geq 0.3$ with $N = 122$.

The correlation is better in July ($r = 0.7$) with a high number of retrievals ($N = 3291$) compared to both cloudy months: April ($N = 1870$, $r = 0.54$) and March ($N = 476$, $r = 0.49$).

A temporal comparison shows very good results and demonstrates that SEVIRI is able to successfully monitor the aerosol load during the day. With a number of retrievals per day greater than 5, the diurnal cycle of aerosol is also observable. The possibility to follow local or regional aerosol features on a 15 min timescale is illustrated over Europe.

AOT product over land at the 0.6 μm channel of the SEVIRI sensor onboard MSG

E. Bernard et al.

Title Page

Abstract

Introduction

Conclusions

References

Tables

Figures

⏪

⏩

◀

▶

Back

Close

Full Screen / Esc

Printer-friendly Version

Interactive Discussion



The monitoring of the aerosol load over long periods using a daily mean AOT is also possible according to the comparison with the daily AOT in-situ measurements. Moreover, qualitative comparisons with the MODIS level 3 daily product show general consistency between SEVIRI and MODIS over the Europe during an aerosol event coming from the North of Africa and crosses the Europe on several days in July 2006. The SEVIRI product is however much more suitable for local and regional studies than the 1° MODIS product. In addition, direct comparisons with Aeronet retrievals and MODIS level 2 products demonstrate that our algorithm compare very well with Aeronet and sometimes better than MODIS while capturing the diurnal variability of aerosol load in a qualitative way that is inaccessible to polar orbiting sensors such as MODIS.

It must be acknowledged that our AOT SEVIRI product currently suffers from some drawbacks due to difficulties in cloud masking which are related to the spatial resolution of SEVIRI (from 3 to 5 km) that does not allow to detect the small scale clouds features. However, cloud mask in remote sensing of aerosols results from a compromise and represents a permanent effort improvement (Kaufman et al., 2005; Frey et al., 2008; Saunders and Kriebel, 1988; Heidinger et al., 2002; Simpson et al., 2001; Trishchenko and Radkevich, 2009; Huo and Lu, 2009; Hagolle et al., 2005).

Another weakness of our algorithm is the difficulty to properly estimate the surface reflectance in specific conditions. This is the case for desert surfaces as well as in specific geometric conditions over vegetation (“hot spot” configuration). Solving these problems would require to use theoretical model of BRDF (e.g., Roujean et al., 1992) or estimate the surface reflectance from other sensors like MODIS or POLDER onboard Low Earth Orbit (LEO) satellites. Besides, methods based on IR channels to retrieve an aerosol product over bright surfaces exist (Legrand and N’doumé, 2001; De Paepe and Dewitte, 2009). These could, in combination with our product, contribute to a better monitoring of aerosols from geostationary satellites.

The assumed background aerosol is probably under-estimated over regions with permanent aerosol load. The use of LEO satellites data to improve estimation of the residual on the day used for the reference is currently being explored.

**AOT product over
land at the 0.6 μm
channel of the SEVIRI
sensor onboard MSG**

E. Bernard et al.

[Title Page](#)
[Abstract](#)
[Introduction](#)
[Conclusions](#)
[References](#)
[Tables](#)
[Figures](#)




[Back](#)
[Close](#)
[Full Screen / Esc](#)
[Printer-friendly Version](#)
[Interactive Discussion](#)


Change 2007: The Physical Science Basis. Contribution of Working Group I to the Fourth Assessment Report of the Intergovernmental Panel on Climate Change, edited by: Solomon, S., Qin, D., Manning, M., Chen, Z., Marquis, M., Averyt, K. B., Tignor, M., and Miller, H. L., Cambridge University Press, Cambridge, United Kingdom and New York, NY, USA, 2007.

3150

Fraser, R. S. and Kaufman, Y. J.: The relative importance of aerosol scattering and absorption in remote-sensing, *IEEE T. Geosci. Remote Sens.*, 23, 625–633, 1985. 3152

Frey, R. A., Ackerman, S. A., Liu, Y., Strabala, K. I., Zhang, H., Key, J. R., and Wang, X.: Cloud Detection with MODIS. Part I: Improvements in the MODIS Cloud Mask for Collection 5, *J. Atmos. Oc. Tech.*, 25, 1057–1072, doi:10.1175/2008JTECHA1052.1, 2008. 3175

Ghan, S., Laulainen, N., Easter, R., Wagener, R., Nemesure, S., Chapman, E., Zhang, Y., and Leung, R.: Evaluation of aerosol direct radiative forcing in MIRAGE, *J. Geophys. Res.*, 106, 5295–5316, doi:10.1029/2000JD900502, 2001. 3150

Govaerts, Y. and Clerici, M.: MSG-1/SEVIRI Solar Channels Calibration Commissioning Activity Report, EUMETSAT, EUM/MSG/TEN/04/0024, 2004. 3155

Govaerts, Y. M., Wagner, S., Lattanzio, A., and Watts, P.: Joint retrieval of surface reflectance and aerosol optical depth from MSG/SEVIRI observations with an optimal estimation approach: 1. Theory, *J. Geophys. Res.*, 115, D02203, doi:10.1029/2009JD011779, 2010. 3151

Grosso, N., Ferreira, F., and Mesquita, S.: Chapter 3.1 Improvement in particles (PM10) urban air quality mapping interpolation using remote sensing data, in: *Air Pollution Modeling and Its Application XVIII*, edited by: Borrego, C. and Renner, E., vol. 6 of *Developments in Environmental Sciences*, 265–274, Elsevier, doi:10.1016/S1474-8177(07)06031-7, 2007. 3150

Guerrieri, L., Corradini, S., Pugnaghi, S., and Santangelo, R.: An aerosol optical thickness retrieval algorithm for Meteosat Second Generation (MSG) data over land: applications to the Mediterranean area, in: *Society of Photo-Optical Instrumentation Engineers (SPIE) Conference Series*, vol. 6745, 2007. 3151

Hagolle, O., Lobo, A., Maisongrande, P., Cabot, F., Duchemin, B., and Pereyra, A. D.: Quality assessment and improvement of temporally composited products of remotely sensed imagery by combination of VEGETATION 1 and 2 images, *Remote Sens. Env.*, 94, 172–186, doi:10.1016/j.rse.2004.09.008, 2005. 3175

Hansen, J., Sato, M., and Ruedy, R.: Radiative forcing and climate response, *J. Geophys. Res.*, 102, 6831–6864, doi:10.1029/96JD03436, 1997. 3150

**AOT product over
land at the 0.6 μm
channel of the SEVIRI
sensor onboard MSG**

E. Bernard et al.

[Title Page](#)
[Abstract](#)
[Introduction](#)
[Conclusions](#)
[References](#)
[Tables](#)
[Figures](#)
[⏪](#)
[⏩](#)
[◀](#)
[▶](#)
[Back](#)
[Close](#)
[Full Screen / Esc](#)
[Printer-friendly Version](#)
[Interactive Discussion](#)


doi:10.1029/2006JD007811, 2007. 3164, 3168

Levy, R. C., Leptoukh, G. G., Kahn, R., Zubko, V., Gopalan, A., and Remer, L. A.: A Critical Look at Deriving Monthly Aerosol Optical Depth From Satellite Data, *IEEE T. Geosc. Remote Sens.*, 47, 2942–2956, doi:10.1109/TGRS.2009.2013842, 2009. 3172

5 Lim, H. S., MatJafri, M. Z., and Abdullah, K.: Retrieval of Air Quality using a newly simulated algorithm from aerosol optical depth, *Map Asia Conference*, 2004. 3150

Lohmann, U. and Feichter, J.: Global indirect aerosol effects: a review, *Atmos. Chem. Phys.*, 5, 715–737, doi:10.5194/acp-5-715-2005, 2005. 3149

Lohmann, U., Rotstajn, L., Storelmo, T., Jones, A., Menon, S., Quaas, J., Ekman, A. M. L.,
10 Koch, D., and Ruedy, R.: Total aerosol effect: radiative forcing or radiative flux perturbation?, *Atmos. Chem. Phys.*, 10, 3235–3246, doi:10.5194/acp-10-3235-2010, 2010. 3150

Moulin, C., Lambert, C. E., Dulac, F., and Dayan, U.: Control of atmospheric export of dust from North Africa by the North Atlantic Oscillation, *Nature*, 387, 691–694, 1997. 3151

Muller, J.: MSG Level 1.5 Image Data Description, EUMETSAT, technical document number
15 EUM/MSG/ICD/105, 2007. 3152

Omar, A. H., Won, J., Winker, D. M., Yoon, S., Dubovik, O., and McCormick, M. P.: Development of global aerosol models using cluster analysis of Aerosol Robotic Network (AERONET) measurements, *J. Geophys. Res.*, 110, D10S14, doi:10.1029/2004JD004874, 2005. 3152,
3160

20 Paepe, B. D., Ignatov, A., Dewitte, S., and Ipe, A.: Aerosol retrieval over ocean from SEVIRI for the use in GERB Earth's radiation budget analyses, *Remote Sens. Env.*, 112, 2455–2468, 2008. 3176

Platnick, S., King, M. D., Ackerman, S. A., Menzel, W. P., Baum, B. A., Riedi, J. C., and Frey, R. A.: The MODIS cloud products: algorithms and examples from Terra, *IEEE T. Geosc. Remote Sens.*, 41, 459–473, doi:10.1109/TGRS.2002.808301, 2003. 3155
25

Popp, C., Hausser, A., Foppa, N., and Wunderle, S.: Remote sensing of aerosol optical depth over central Europe from MSG-SEVIRI data and accuracy assesment with ground-based AERONET measurements, *J. Geophys. Res.*, 112, D24S11, doi:10.1029/2007JD008423, 2007. 3151, 3159

30 Quaas, J., Boucher, O., Bellouin, N., and Kinne, S.: Satellite-based estimate of the direct and indirect aerosol climate forcing, *J. Geophys. Res.*, 113, D05204, doi:10.1029/2007JD008962, 2008. 3150

Ramon, D. and Santer, R.: Operational Remote Sensing of Aerosols over Land to Account for

AOT product over land at the 0.6 μm channel of the SEVIRI sensor onboard MSG

E. Bernard et al.

[Title Page](#)
[Abstract](#)
[Introduction](#)
[Conclusions](#)
[References](#)
[Tables](#)
[Figures](#)




[Back](#)
[Close](#)
[Full Screen / Esc](#)
[Printer-friendly Version](#)
[Interactive Discussion](#)


Directional Effects, *Appl. Opt.*, 40, 3060–3075, 2001. 3154

Remer, A. L., Kaufman, Y. J., Tanré, D., Matoo, S., Chu, D. A., Martins, J. V., Li, R. R., Ichoku, C., Levy, R. C., Kleidman, R. G., Eck, T. F., Vermote, E., and Holben, B. N.: The MODIS Aerosol Algorithm, Products and Validation, *J. Atmos. Sci.*, 62, 947–973, 2005. 3164, 3168

Rohen, G. J., von Hoyningen-Huene, W., Kokhanovsky, A., Dinter, T., Vountas, M., and Burrows, J. P.: Retrieval of aerosol mass load (PM₁₀) from MERIS/Envisat top of atmosphere spectral reflectance measurements over Germany, *Atmos. Meas. Tech.*, 4, 523–534, doi:10.5194/amt-4-523-2011, 2011. 3150

Roujean, J.-L., Leroy, M., and Deschamps, P.-Y.: A Bidirectional Reflectances Model of the Earth's Surface for the Correction of Remote Sensing Data, *J. Geophys. Res.*, 97, 20455–20468, 1992. 3175

Santer, J. R., Carrere, V., and Dubuisson, P.: Atmospheric correction over land for MERIS, *Int. J. Remote Sens.*, 20, 1819–1840, 1999. 3154

Saunders, R. W. and Kriebel, K. T.: An improved method for detecting clear sky and cloudy radiances from AVHRR data, *Int. J. Remote Sens.*, 9, 123–150, doi:10.1080/01431168808954841, 1988. 3175

Schulz, M., Textor, C., Kinne, S., Balkanski, Y., Bauer, S., Bernsten, T., Berglen, T., Boucher, O., Dentener, F., Guibert, S., Isaksen, I. S. A., Iversen, T., Koch, D., Kirkevåg, A., Liu, X., Montanaro, V., Myhre, G., Penner, J. E., Pitari, G., Reddy, S., Seland, Ø., Stier, P., and Takemura, T.: Radiative forcing by aerosols as derived from the AeroCom present-day and pre-industrial simulations, *Atmos. Chem. Phys.*, 6, 5225–5246, doi:10.5194/acp-6-5225-2006, 2006. 3150

Schwartz, S. E. and Slingo, A.: Enhanced shortwave cloud radiative forcing due to anthropogenic aerosols, NASA STI/Recon Technical Report N, 95, 34214–34261, 1995. 3149

Seinfeld, J. H. and Pandis, S. N.: *Atmospheric chemistry and physics. From air pollution to climate change*, John Wiley and Sons, New York, 1997. 3150

Sifikis, N. I.: Quantitative mapping of air pollution density using Earth observations: a new processing method and application to an urban area, *Int. J. Remote Sens.*, 19, 3289–3300, doi:10.1080/014311698213975, 1998. 3150, 3176

Simpson, J., McIntire, T., Stitt, J., and Hufford, G.: Improved cloud detection in AVHRR daytime and nighttime scenes over the ocean, in: *Society of Photo-Optical Instrumentation Engineers (SPIE) Conference Series*, edited by: Russell, J. E., Schaefer, K., and Lado-Bordowsky, O., vol. 4168, 48–55, 2001. 3175

AOT product over land at the 0.6 μm channel of the SEVIRI sensor onboard MSG

E. Bernard et al.

[Title Page](#)
[Abstract](#)
[Introduction](#)
[Conclusions](#)
[References](#)
[Tables](#)
[Figures](#)
[Back](#)
[Close](#)
[Full Screen / Esc](#)
[Printer-friendly Version](#)
[Interactive Discussion](#)


- Thieuleux, F., Moulin, C., Breon, F. M., Maignan, F., Poitou, J., and Tanré, D.: Remote sensing of aerosol over the oceans using MSG/SEVIRI imagery, *Ann. Geophys.*, 23, 1–8, 2005. 3151, 3161
- Trishchenko, A. P. and Radkevich, A. V.: Improving the Cloud Mask For MERIS/ENVISAT Imagery Received Over Canada, AGU Fall Meeting Abstracts, pp. F289+, 2009. 3175
- Twomey, S.: Aerosols, clouds and radiation, *Atmos. Env.*, 25, 2435–2442, 1991. 3149
- Vermote, E., Tanré, D., Deuze, J.-L., Herman, M., and Morcrette, J. J.: Second Simulation of the Satellite in the Solar Spectrum, 6S: An overview, *IEEE T. Geosc. Remote Sens.*, 35, 675–686, 1997. 3154
- Vermote, E. F., El Saleous, N., Justice, C. O., Kaufman, Y. J., Privette, J. L., Remer, L., Roger, J. C., and Tanré, D.: Atmospheric correction of visible to middle-infrared EOS-MODIS data over land surfaces: Background, operational algorithm and validation, *J. Geophys. Res.*, 102, 17131–17142, doi:10.1029/97JD00201, 1997. 3154, 3157
- Wagner, S. C., Govaerts, Y. M., and Lattanzio, A.: Joint retrieval of surface reflectance and aerosol optical depth from MSG/SEVIRI observations with an optimal estimation approach: 2. Implementation and evaluation, *J. Geophys. Res.*, 115, D02204, doi:10.1029/2009JD011780, 2010. 3151
- Wang, J. and Christopher, S. A.: Intercomparison between satellite-derived aerosol optical thickness and $PM_{2.5}$ mass: Implications for air quality studies, *Geophys. Res. L.*, 30, 2095, doi:10.1029/2003GL018174, 2003. 3150
- Wayne, R.: *An Introduction to the Chemistry of the Atmospheres of Earth, the Planets, and their Satellites*, Oxford University Press, Oxford, 2000. 3150
- Whitby, K.: Physical characterization of aerosol, in: *Methods and standards for Environmental measurement*, 165–173, proceedings of 8th IMR Symposium, 1976. 3149

AOT product over land at the 0.6 μm channel of the SEVIRI sensor onboard MSG

E. Bernard et al.

Table 1. Physical and optical parameters of the aerosol models used in the algorithm (Omar et al., 2005). Models are: MA = Moderately Absorbing; UI = Urban-Industrial non absorbing; SM = Smoke; SD = Spheroidal Dust. Number of each model is reported in the first column. The characteristics, given for both fine and coarse mode, are the median radius of the volume size distribution (R_v) in μm , the neperian logarithm of σ_v representing the standard deviation of this median radius, the volume of particles per cross section of the atmospheric column (V_o) and the complex refractive index (n) at 0.6 μm . The extinction fraction of each mode is also given (F). The WMO continental model is from Lenoble and Brogniez (1984) (see text).

#	mode	R_v (μm)	σ_v	$V_o(dV/dlnr)$ [$\mu\text{m}^3/\mu\text{m}^2$]	n	F
1	WMO –	–	–	–	–	–
2	MA Acc.	0.15	0.42	0.096	1.43–0.007i	0.82
	Coarse	3.26	0.77	0.092	1.43–0.007i	0.18
3	UI Acc.	0.18	0.43	0.096	1.42–0.007i	0.89
	Coarse	3.4	0.83	0.06	1.42–0.007i	0.11
4	SM Acc.	0.14	0.42	0.092	1.51–0.02i	0.91
	Coarse	4.0	0.76	0.064	1.51–0.02i	0.09
5	SD Acc.	0.14	0.76	0.087	1.48–0.0018i	0.83
	Coarse	2.2	0.55	0.068	1.48–0.0018i	0.17

Title Page

Abstract

Introduction

Conclusions

References

Tables

Figures

◀

▶

◀

▶

Back

Close

Full Screen / Esc

Printer-friendly Version

Interactive Discussion



Table 2. Coordinates and description of the 43 AERONET stations used for the validation. The country of each station is indicated in parenthesis: FR. = France, DE. = Germany, PT. = Portugal, ES. = Spain, GR. = Greece, RU. = Russia, MD. = Moldova, Republic Of, IT. = Italy, BE. = Belgium, CH. = Switzerland, NL. = The Netherlands, PL. = Poland, UA. = Ukraine, SE. = Sweden, EE. = Estonia, BY. = Belarus, UK. = United Kingdom.

Stations	Lat.(°)	Lon.(°)	Stations	Lat.(°)	Lon.(°)
Avignon (FR.)	43.9N	4.88E	La Crau (FR.)	43.58N	4.8E
Barcelona (ES.)	41.39N	2.12E	Laegeren (CH.)	47.48N	8.35E
Belsk (PL.)	51.84N	20.79E	Lecce University (IT.)	40.33N	18.11
Brussels (BE.)	50.78N	4.35E	Le Fauga (FR.)	43.38N	1.28E
Cabauw (NL.)	51.97N	4.93E	Lille (FR.)	50.61N	3.14E
Cabo Da Roca (PT.)	38.78N	9.5W	Mainz (DE.)	50N	8.3E
Carpentras (FR.)	44.08N	5.06E	Minsk (BY.)	53.92N	27.6E
Chilbolton (UK.)	51.14N	1.44W	Modena (IT.)	44.63N	10.94E
Davos (CH.)	46.8N	9.84E	Moldova (MD.)	47N	28.81E
Dunkerque (FR.)	51.03N	2.37E	Moscow MSU MO (RU.)	55.7N	37.51E
Epanomi (GR.)	40.37N	22.98E	OHP Observatory (FR.)	43.93N	5.7E
Evora (PT.)	38.57N	7.9W	Oostende (BE.)	51.22N	2.92E
Fontainebleau (FR.)	48.4N	2.68E	Palaiseau (FR.)	48.7N	2.2E
Forth crete (GR.)	35.33N	25.28E	Palencia (ES.)	41.99N	4.51W
Granada (ES.)	37.16N	3.6W	Paris (FR.)	48.87N	2.33E
Hamburg (DE.)	53.57N	9.73E	Rome Tor Vergata (IT.)	41.84N	12.65E
Helgoland (DE.)	54.18N	7.89E	Sevastopol (UA.)	44.61N	33.52E
IMAA Potenza (IT.)	40.6N	15.72E	SMHI (SE.)	58.58N	16.15E
Ispra (IT.)	45.8N	8.63E	Thessaloniki (GR.)	40.63N	22.96E
The Hague (NL.)	52.11N	4.33E	Toravere (EE.)	58.25N	26.46E
Toulon (FR.)	43.14N	6E	Venise (IT.)	45.31N	12.5E
Villefranche (FR.)	43.98N	7.33E			

AOT product over land at the 0.6 μm channel of the SEVIRI sensor onboard MSG

E. Bernard et al.

Title Page

Abstract

Introduction

Conclusions

References

Tables

Figures

◀

▶

◀

▶

Back

Close

Full Screen / Esc

Printer-friendly Version

Interactive Discussion

AOT product over land at the 0.6 μm channel of the SEVIRI sensor onboard MSG

E. Bernard et al.

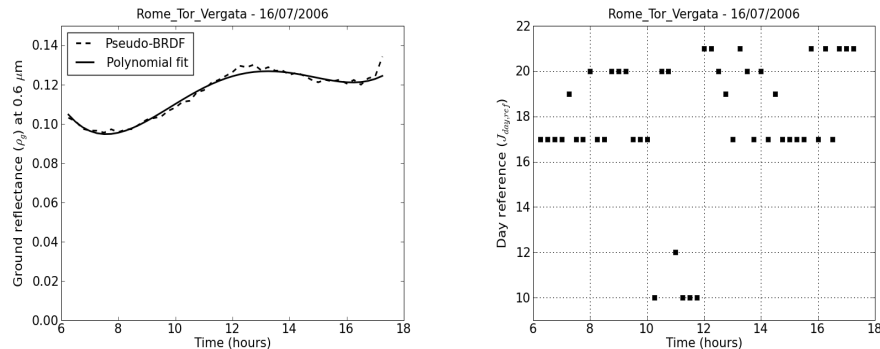


Fig. 1. Rome site on the 16 July 2006. (*left*) Ground reflectance (ρ_g) at 0.6 μm : the pseudo-BRDF (or reference reflectance) based on the 14 days minimum (black dashed curve) and the fourth degree polynomial fit (black curve). (*right*) $J_{\text{day,ref}}$: the day with the smallest L1B reflectance at VIS06 channel.

[Title Page](#)
[Abstract](#)
[Introduction](#)
[Conclusions](#)
[References](#)
[Tables](#)
[Figures](#)
[⏪](#)
[⏩](#)
[◀](#)
[▶](#)
[Back](#)
[Close](#)
[Full Screen / Esc](#)
[Printer-friendly Version](#)
[Interactive Discussion](#)

AOT product over land at the 0.6 μm channel of the SEVIRI sensor onboard MSG

E. Bernard et al.

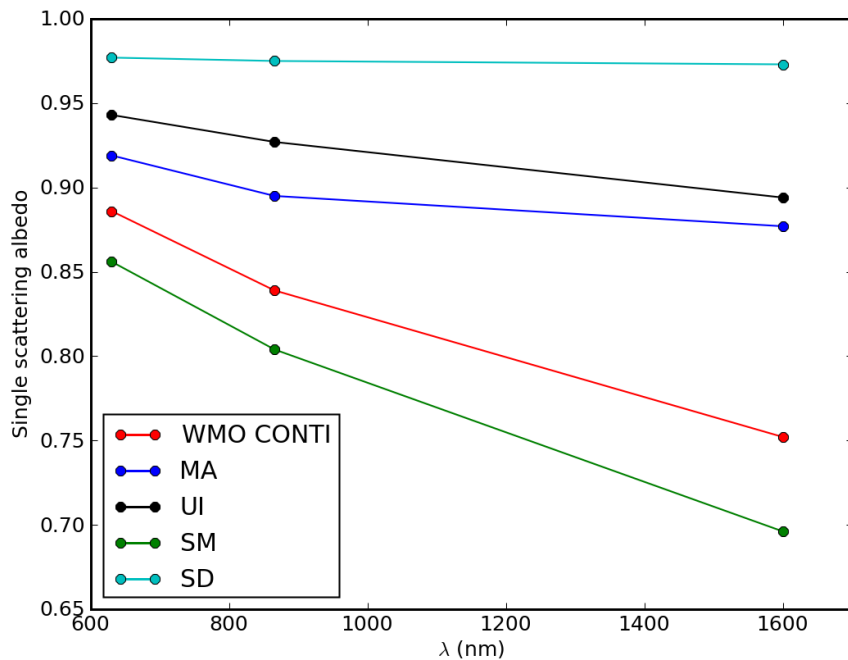


Fig. 2. Single scattering albedo (ω_0) for the 5 aerosol models used by the algorithm to retrieve the AOT at 0.6 μm .

[Title Page](#)[Abstract](#)[Introduction](#)[Conclusions](#)[References](#)[Tables](#)[Figures](#)[◀](#)[▶](#)[◀](#)[▶](#)[Back](#)[Close](#)[Full Screen / Esc](#)[Printer-friendly Version](#)[Interactive Discussion](#)

AOT product over land at the 0.6 μm channel of the SEVIRI sensor onboard MSG

E. Bernard et al.

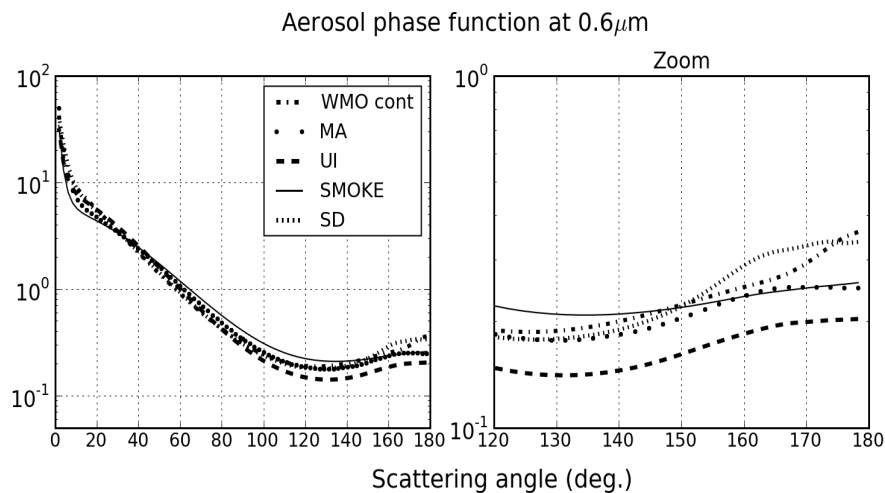


Fig. 3. Aerosol phase function for each 5 models at 0.6 μm between 0° and 180° (left). A zoom for the backscattering part (from 120° to 180°) is also plotted (right).

AOT product over land at the 0.6 μm channel of the SEVIRI sensor onboard MSG

E. Bernard et al.

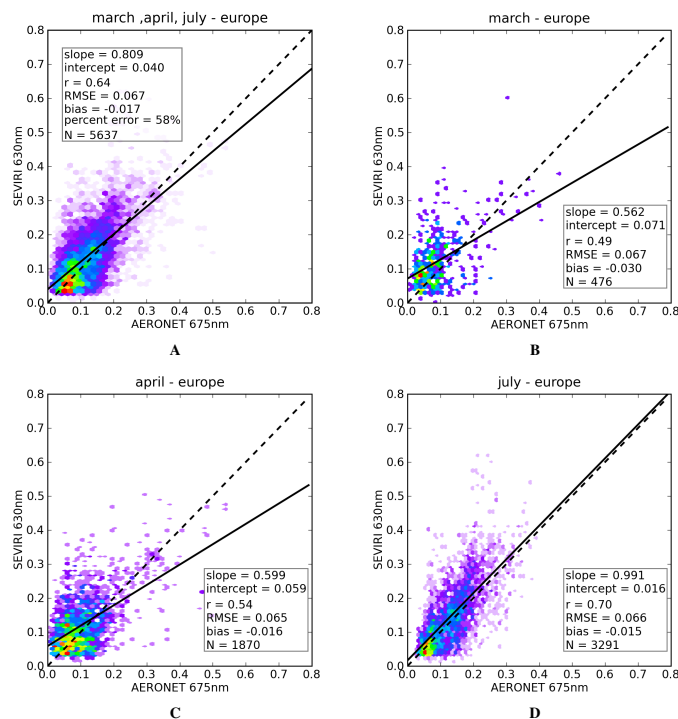


Fig. 4. Density graph of AOT SEVIRI against AERONET at 0.6 μm for European stations for the 3 months: March, April and July 2006 (**A**). The linear regression (black line) and the one-to-one curve (black dashed line) are plotted. The parameters of the linear regression are indicated on the graph. Individual validation for the 3 months separately are also plotted: March (**B**), April (**C**) and July (**D**).

[Title Page](#)
[Abstract](#)
[Introduction](#)
[Conclusions](#)
[References](#)
[Tables](#)
[Figures](#)
[⏪](#)
[⏩](#)
[◀](#)
[▶](#)
[Back](#)
[Close](#)
[Full Screen / Esc](#)
[Printer-friendly Version](#)
[Interactive Discussion](#)

AOT product over land at the 0.6 μm channel of the SEVIRI sensor onboard MSG

E. Bernard et al.

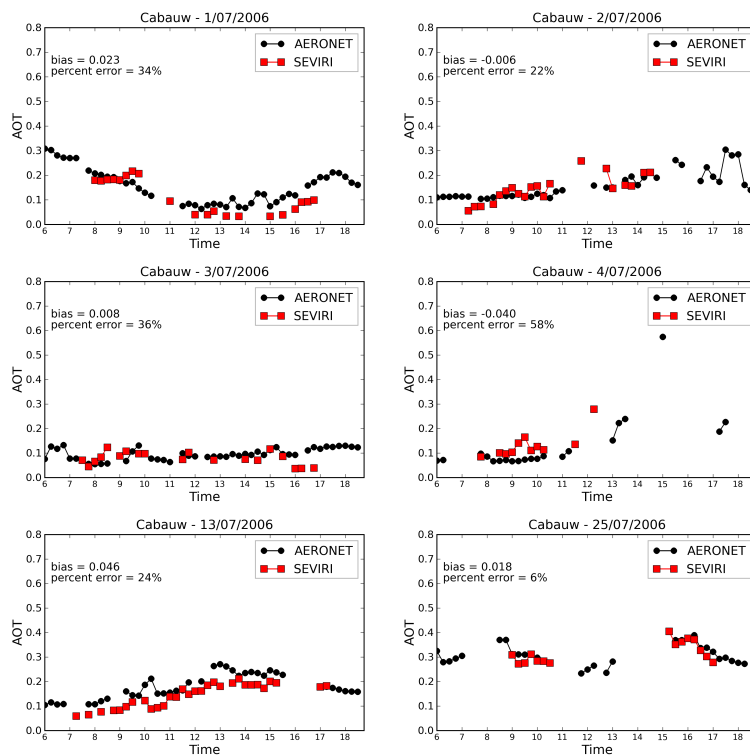


Fig. 5. Temporal evolution of the Aerosol Optical Thickness above Cabauw for some days in July 2006: from 1 to 4 and on 13 and 25. The black line is AERONET and the red line is SEVIRI. The time scale is from 06:00 to 18:00 UTC and the AOT scale is from 0 to 0.7. The mean bias and the mean relative bias are indicated on each plot.

[Title Page](#)
[Abstract](#)
[Introduction](#)
[Conclusions](#)
[References](#)
[Tables](#)
[Figures](#)
[⏪](#)
[⏩](#)
[⏴](#)
[⏵](#)
[Back](#)
[Close](#)
[Full Screen / Esc](#)
[Printer-friendly Version](#)
[Interactive Discussion](#)

**AOT product over
land at the 0.6 μm
channel of the SEVIRI
sensor onboard MSG**

E. Bernard et al.

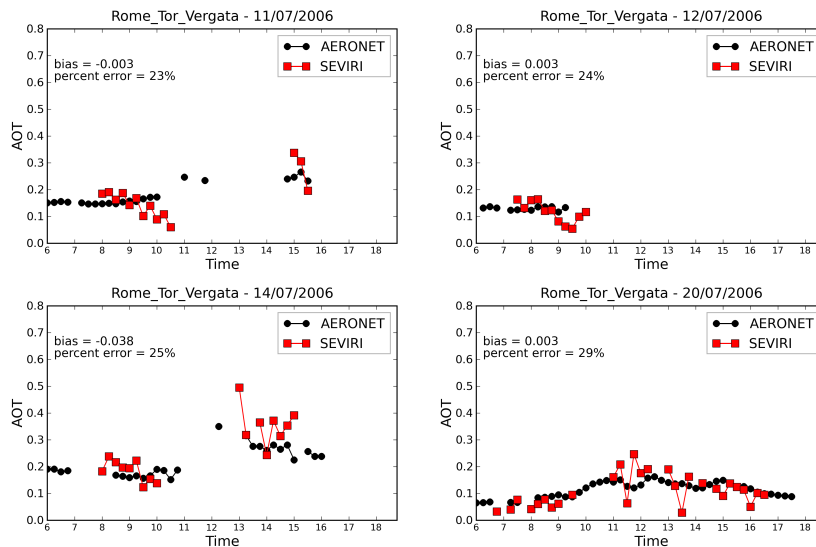


Fig. 6. Same as Fig. 5 but for Rome Tor Vergata station for days: 11, 12, 14 and 20 on July 2006.

[Title Page](#)[Abstract](#)[Introduction](#)[Conclusions](#)[References](#)[Tables](#)[Figures](#)[◀](#)[▶](#)[◀](#)[▶](#)[Back](#)[Close](#)[Full Screen / Esc](#)[Printer-friendly Version](#)[Interactive Discussion](#)

AOT product over land at the 0.6 μm channel of the SEVIRI sensor onboard MSG

E. Bernard et al.

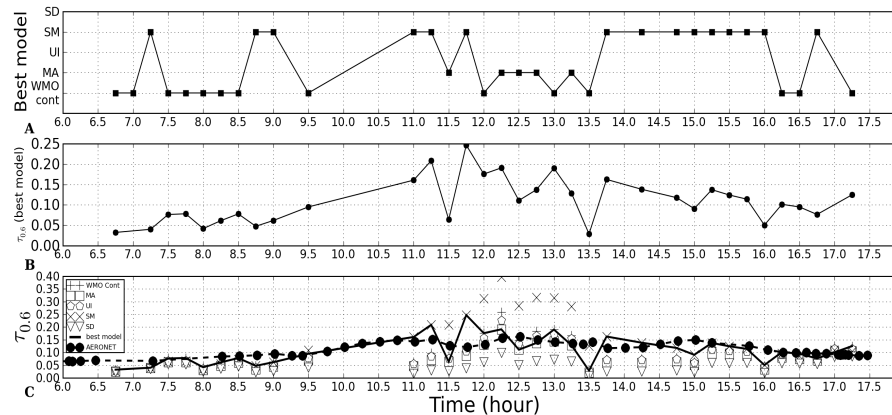


Fig. 7. Temporal evolution of aerosols parameters retrieved over Rome on the 20 July 2006. **(A)** Best aerosol model retrieved by the algorithm (see Table 1). **(B)** SEVIRI best model Aerosol optical thickness at 0.6 μm . **(C)** Aerosol optical thickness for each model (symbol): WMO continental (plus), Moderately Absorbing (square), Urban Industrial (pentagon), Smoke (cross), Spheroidal Dust (triangle). AOT best model (black line) and AOT AERONET (black circle).

**AOT product over
land at the 0.6 μm
channel of the SEVIRI
sensor onboard MSG**

E. Bernard et al.

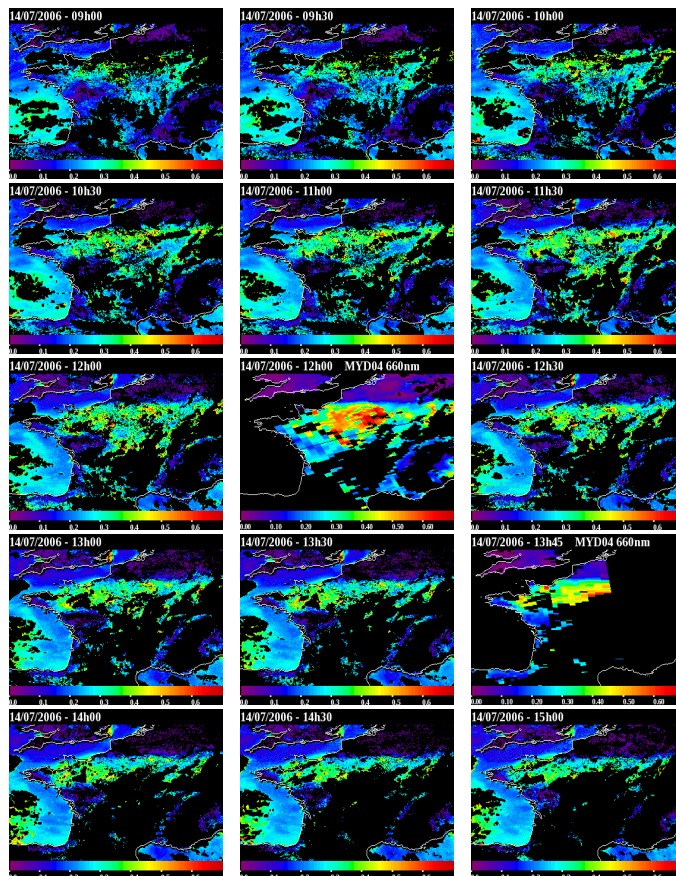


Fig. 8. Maps of aerosol optical thickness retrieved by SEVIRI at 0.6 μm for the 14 July 2006 above France, Benelux and West Germany from 09:00 to 15:00. Two MODIS AQUA aerosol optical thickness level 2 maps are also showed at 12:00 and 13:45. The color scale is from 0 to 0.7.

[Title Page](#)[Abstract](#)[Introduction](#)[Conclusions](#)[References](#)[Tables](#)[Figures](#)[⏪](#)[⏩](#)[◀](#)[▶](#)[Back](#)[Close](#)[Full Screen / Esc](#)[Printer-friendly Version](#)[Interactive Discussion](#)

AOT product over land at the 0.6 μm channel of the SEVIRI sensor onboard MSG

E. Bernard et al.

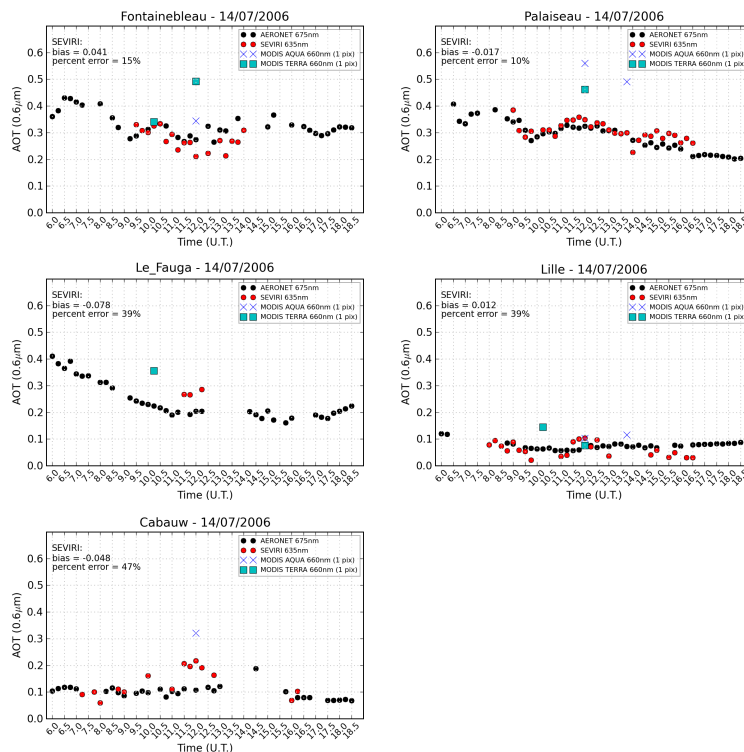


Fig. 9. Temporal evolution of the Aerosol Optical Thickness above Fontainebleau, Palaiseau, Le Fauga (near Toulouse), Lille and Cabauw for the 14 July 2006. The black dots are AERONET, the red dots are SEVIRI and the blue crosses and cyan squares are for MODIS AQUA and TERRA at 660nm. The mean bias and the mean relative bias between AERONET and SEVIRI are indicated on each plot. The SEVIRI and MODIS pixels are the ones geolocated with the AERONET station. The time scale is from 06:00 to 18:45 UTC and the AOT scale is from 0 to 0.7.

Title Page

Abstract

Introduction

Conclusions

References

Tables

Figures

◀

▶

◀

▶

Back

Close

Full Screen / Esc

Printer-friendly Version

Interactive Discussion

**AOT product over
land at the 0.6 μm
channel of the SEVIRI
sensor onboard MSG**

E. Bernard et al.

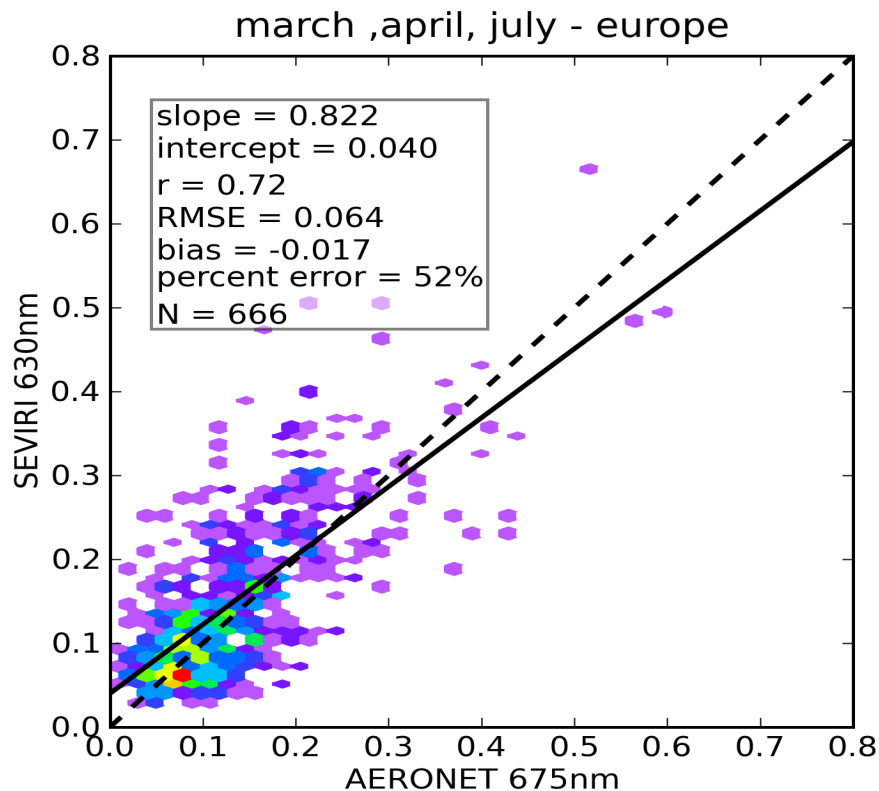


Fig. 10. Density graph of the daily SEVIRI and AERONET AOT at 0.6 μm for European stations for the 3 months of interest (March, April and July 2006). The linear regression is plotted and the results of this regression are indicated on the graph.

Title Page

Abstract

Introduction

Conclusions

References

Tables

Figures

◀

▶

◀

▶

Back

Close

Full Screen / Esc

Printer-friendly Version

Interactive Discussion

AOT product over land at the 0.6 μm channel of the SEVIRI sensor onboard MSG

E. Bernard et al.

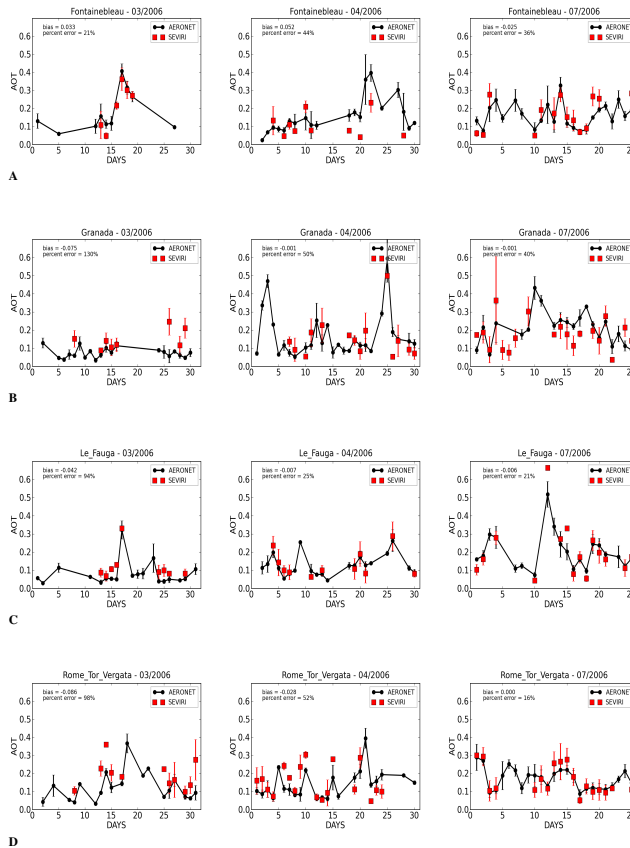


Fig. 11. Temporal evolution of the daily averaged AOT for 4 AERONET stations in March, April and July 2006. Stations are Fontainebleau (**A**), Granada (**B**), Le Fauga (**C**) and Rome Tor Vergata (**D**). The black curve is the AOT AERONET and the red one is the AOT SEVIRI. The standard deviations are also plotted. The averages are made independently for AERONET and SEVIRI.

Title Page

Abstract Introduction

Conclusions References

Tables Figures

⏪ ⏩

⏴ ⏵

Back Close

Full Screen / Esc

Printer-friendly Version

Interactive Discussion

**AOT product over
land at the 0.6 μm
channel of the SEVIRI
sensor onboard MSG**

E. Bernard et al.

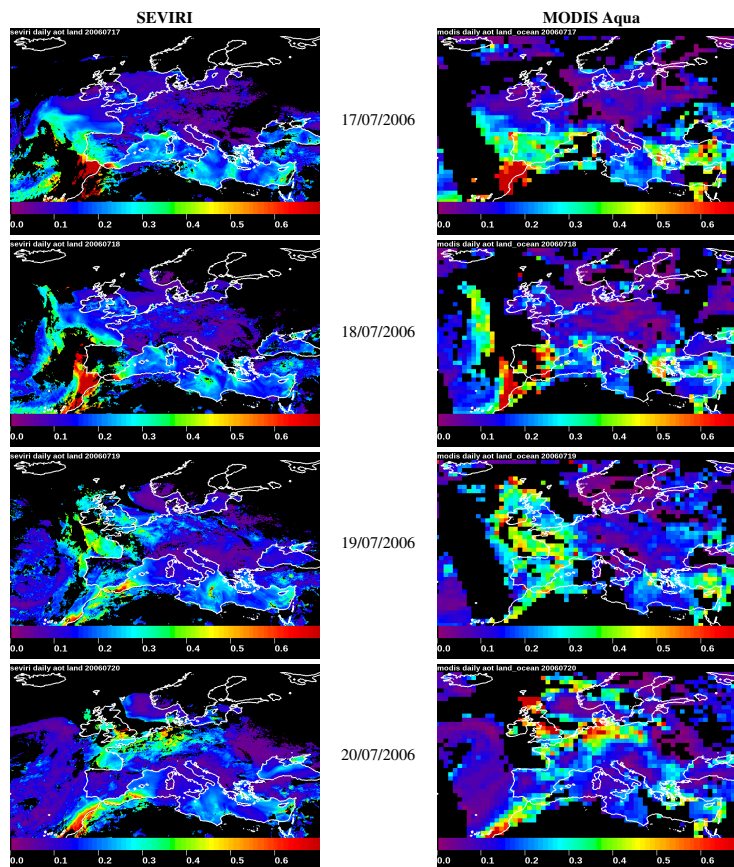


Fig. 12. Daily AOT maps at 0.6 μm above Europe for SEVIRI (left) and MODIS (right) sensors. The spatial resolution of SEVIRI is $0.1^\circ \times 0.1^\circ$ while it is 1° for MODIS. Days presented are from the 17 (top) to the 20 (bottom) July 2006. The color scale is from 0 to 0.7.

Title Page

Abstract

Introduction

Conclusions

References

Tables

Figures

◀

▶

◀

▶

Back

Close

Full Screen / Esc

Printer-friendly Version

Interactive Discussion

AOT product over land at the 0.6 μm channel of the SEVIRI sensor onboard MSG

E. Bernard et al.

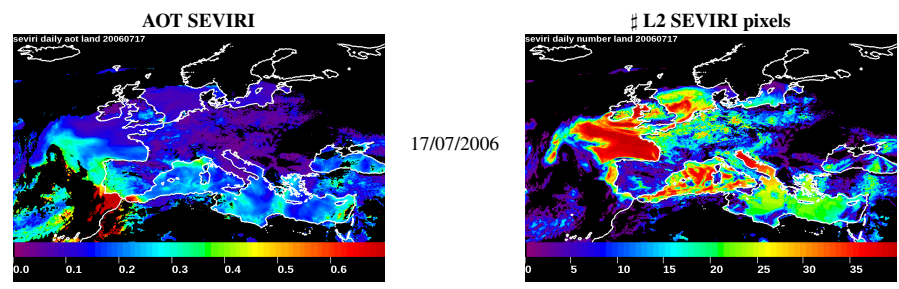


Fig. 13. Daily SEVIRI maps above Europe on the 17 July 2006: on the left the AOT at 0.6 μm and on the right the quantity of L2 pixels to process the AOT daily average.

Title Page

Abstract Introduction

Conclusions References

Tables Figures

⏪ ⏩

◀ ▶

Back Close

Full Screen / Esc

Printer-friendly Version

Interactive Discussion

